

# Beam energy dependence of transverse momentum distribution and elliptic flow in Au-Au collisions using HYDJET++ model

Satya Ranjan Nayak<sup>1,\*</sup>, Saraswati Pandey<sup>1,†</sup> and B. K. Singh<sup>1,2‡</sup>

<sup>1</sup>*Department of Physics, Institute of Science,  
Banaras Hindu University (BHU),  
Varanasi, 221005, INDIA.*

<sup>2</sup>*Discipline of Natural Sciences,  
PDPM Indian Institute of Information Technology Design & Manufacturing,  
Jabalpur-482005, India  
(Dated: May 7, 2024)*

In this work, we present the transverse momentum spectra and elliptic flow ( $v_2$ ) of  $\pi^\pm, k^\pm, p$  and  $\bar{p}$  in Au-Au collisions at  $\sqrt{s_{NN}} = 62.4, 39.0, 27.0, 19.6$  and  $11.5$  GeV using HYDJET++ model. For each beam energy the transverse momentum spectra are shown in four centrality classes at mid rapidity  $|y| \leq 0.1$  and for elliptic flow ( $v_2$ ) we have shown results for minimum bias events. We have performed a qualitative comparison between the hard and soft processes at different beam energies. The HYDJET++ model calculations for particle ratios,  $p_T$  spectra, and  $v_2$  agree well with the available experimental data. The HYDJET++ parameters like baryonic and strangeness chemical potential, and chemical and thermal freeze-out temperature vary with collision energy. Azimuthal spatial anisotropy ( $\epsilon$ ) and azimuthal momentum anisotropy ( $\delta$ ) decrease with collision energy which leads to a smaller value of  $v_2$  at lower collision energies. Furthermore, the hadrons containing strange quarks tend to have smaller values of spatial and momentum anisotropy than the non-strange hadrons.

## I. INTRODUCTION

Heavy Ion collision experiments at RHIC and LHC have a common objective to study an exotic state of matter called Quark Gluon Plasma (QGP) formed at extreme temperature and density which is strong enough to deconfine the quarks and gluons [1–3]. One of the plausible approaches to study such a de-confined medium is to vary the collision energy and study its signals [4] like elliptic flow [5], jet quenching [6], strangeness abundance [7, 8],  $j/\psi$  suppression [9], etc. Such an approach can be used for scanning the phase diagram of QCD as both temperature and chemical potential can be changed by varying collision energy [10–12]. Another advantage of using such a method is the possibility of finding the QCD critical point, which marks the end of the first-order phase transition [13, 14]. The critical point can be identified by enhanced fluctuations in conserved quantities like baryon number, charge, strangeness, etc [15–17].

An experimental approach to study the collision systems at wide range of beam energies was made in the RHIC Beam Energy Scan (BES) program [18–20] which explored thirteen beam energies from the top RHIC energy of  $\sqrt{s_{NN}} = 200$  GeV to the lowest energy of 3 GeV. A series of experiments under the BES program tried to find the phase boundary and critical point by looking for the signals of QGP at different collision energies. The BES program generated a large volume of experimental data for different important observables like  $p_T$  spectra,

$v_2$ , higher moments, etc for different collision energies. The highest energy of the BES program (i.e. 200 GeV) has been studied widely, while more phenomenological studies need to be performed for these smaller systems to study their behavior and mechanism of particle production. Furthermore, a qualitative difference between experimental data and theoretical model calculations or a deviation from the trend of model parameters at a particular beam energy could suggest a change in the particle production mechanism. Hence, the beam energy dependence of different signals and the model parameters need to be studied using a suitable theoretical model.

Some theoretical attempts were made before to predict the beam energy dependence of signals like  $v_2$  using models like AMPT, UrQMD, etc [21, 22]. A hydrodynamical treatment can be used to get a new insight into this problem. The theoretical model we chose to employ is the HYDJET++ model. It gives the option to study the collision systems as a combination of soft QCD processes (HYDrodynamics) and hard QCD processes (JETs). Our main goal is to study the bulk properties of the QGP medium produced in lower collision energies such as  $p_T$  spectra, particle multiplicities, and elliptic flow, which are best described by the Monte Carlo event generators. HYDJET++ model has been successful in reproducing the experimental data at LHC energies and the top RHIC energy [23–25]. One of the main distinctions between the top RHIC energy, the LHC energies, and these lower energies is the large values of the chemical potential of these smaller systems. The model needs to be tested at lower collision energies to check the validity and implications of such treatment.

The paper is organized as follows. In section II, we have discussed the HYDJET++ framework. Section III

\* satyanayak@bhu.ac.in

† saraswati.pandey13@bhu.ac.in

‡ bksingh@bhu.ac.in; director@iiitdmj.ac.in

is divided into three sub-sections. In sub-section A, we have discussed the particle ratios and freeze-out parameters. In sub-section B, we have shown the  $p_T$  spectra at different collision energies and discussed the contribution from hard and soft processes. In sub-section C, we have shown the elliptic flow  $v_2$  as a function of  $p_T$  at different collision energies. Finally, in section IV, we have summarised our work.

## II. HYDJET++ MODEL

HYDJET++ is a Monte Carlo Heavy Ion collision event generator that produces particles as a combination of hard and soft processes [24, 26]. The soft part does a detailed treatment of thermal particle production, collective flow, etc. While the hard part deals with jet production, collisional and radiative energy loss, nuclear shadowing, etc.

The hard part of the model is generated by PYQUEN. The initial patron spectra and jet production vertices from binary N-N sub-collisions are generated by PYTHIA 6 [27]. The jets produced in Au-Au collisions are a combination of jets produced from these binary sub-collisions. PYQUEN calculates the rescattering path of partons in the dense QGP medium and the radiative and collisional energy loss. The final hadronization is done according to the Lund string model. The nuclear shadowing for each impact parameter is done according to Glauber-Gribov theory [28].

The soft part of the HYDJET++ is generated on chemical and thermal freeze-out hypersurfaces with  $T_{th}$  and  $T_{ch}$  as the input parameters. A detailed physics framework can be found in the corresponding papers [29, 30]. The momentum distribution of hadrons is given by the equilibrium distribution function:

$$f_i^{eq}(p^{*0}, T, \mu_i, \gamma_s) = \frac{g_i}{\gamma_s^{-n_i^s} \exp([p^{*0} - \mu_i]/T) \pm 1} \quad (1)$$

Where  $p^{*0}$  is the hadron energy in the fluid rest frame,  $g_i = 2J_i + 1$  is the spin degeneracy,  $\gamma^s$  is the strangeness suppression factor, and  $\pm$  takes account of the quantum statistics of a fermion or boson. The particle density at a given  $T_{ch}$  and  $\mu$  is given by

$$\rho_i^{eq}(T, \mu_i) = \frac{g_i}{2\pi^2} m_i^2 T \sum_{k=1}^{\infty} \frac{(\mp)^{k+1}}{k} \exp\left(\frac{k\mu_i}{T}\right) K_2\left(\frac{km_i}{T}\right) \quad (2)$$

where  $m_i$  is the particle mass and  $K_2$  is the modified Bessel's function. Chemical potential  $\mu_i$  of a particle depends on baryon number B, strangeness S, electric charge(Isospin) Q, charm C, etc. However, for this work, we have considered only baryon number, strangeness, and i.e.  $\mu_i = B_i\mu_B + S_i\mu_s + Q_i\mu_Q$ . The baryonic chemical potential and chemical freeze-out temperature for different beam energies are chosen according to the following

equation [12].

$$T(\mu_B) = a - b\mu_B^2 - c\mu_B^4,$$

$$\mu_B(\sqrt{s_{NN}}) = \frac{d}{1 + e\sqrt{s_{NN}}} \quad (3)$$

where,  $a=0.166\pm 0.002$  GeV,  $b=0.139\pm 0.016$  GeV<sup>-1</sup>,  $c=0.053\pm 0.021$  GeV<sup>-3</sup>,  $d=1.308\pm 0.028$  GeV,  $e=0.273\pm 0.008$  GeV<sup>-1</sup>.

The values of  $\mu_s$  are chosen to get the best match with the experimentally observed  $k^-/k^+$ ,  $k^+/\pi^+$  and  $k^-/\pi^-$  ratios and  $p_T$  spectra simultaneously. The value of isospin chemical potential is kept constant for all beam energies ( $\mu_Q = -0.001$  GeV). The particle numbers are fixed after the chemical freeze-out. However, there are some corrections in the number of produced particles due to the decay of short-lived particles. To estimate the particle number densities at thermal freeze-out, the particle ratios at chemical freeze-out are assumed to be the same as thermal freeze-out. The effective pion chemical potential at thermal freeze-out is defined as follows,

$$\frac{\rho_i^{eq}(T^{ch}, \mu_i)}{\rho_\pi^{eq}(T^{ch}, \mu_i^{ch})} = \frac{\rho_i^{eq}(T^{th}, \mu_i^{th})}{\rho_\pi^{eq}(T^{th}, \mu_\pi^{eff})} \quad (4)$$

where,  $\mu_{\pi^+}^{eff}$  is the effective chemical potential of  $\pi^+$  at thermal freeze-out. The values of  $T_{th}$  and  $\mu_{\pi^+}^{eff}$  are chosen to get the best match with  $p_T$  distribution measured in RHIC BES [19]. For this work, we have assumed  $T_{th}$  and  $\mu_{\pi^+}^{eff}$  to be independent of centrality. Assuming Boltzmann approximation in eq. (2) for particles heavier than pions [31], from eq. (2) and eq. (4) the chemical potential of  $i^{th}$  hadron species at thermal freeze-out:

$$\mu_i^{th} = \ln\left(\frac{\rho_i^{eq}(T^{ch}, \mu_i^{ch})}{\rho_i^{eq}(T^{th}, \mu_i = 0)} \frac{\rho_\pi^{eq}(T^{th}, \mu_i^{th})}{\rho_\pi^{eq}(T^{th}, \mu_\pi^{eff})}\right) \quad (5)$$

The longitudinal motion is dominant in the relativistic heavy ion collisions. Hence, the fluid flow four-velocity  $\{u^0(x), \vec{u}(x)\}$  is parameterized in terms of longitudinal ( $z$ ) and transverse ( $r_\perp$ ) flow rapidities

$$\eta^u(x) = \frac{1}{2} \ln \frac{1 + v_z(x)}{1 - v_z(x)} \quad (6)$$

$$\rho^u(x) = \frac{1}{2} \ln \frac{1 + v_\perp(x) \cosh \eta^u(x)}{1 - v_\perp(x) \cosh \eta^u(x)} \quad (7)$$

Where  $v_\perp$  is the magnitude of the transverse component of flow three-velocity  $\vec{v} = \{v_\perp, v_z\} = \{v_\perp \cos \phi^u, v_\perp \sin \phi^u, v_z\}$ , i.e.,

$$u^\mu(x) = \{\cosh \rho^u \cosh \eta^u, \sinh \rho^u \cos \phi^u, \sinh \rho^u \sin \phi^u, \cosh \rho^u \sinh \eta^u\}$$

$$= \{(1 + u_{\perp}^2)^{1/2} \cosh \eta^u, u_{\perp}, (1 + u_{\perp}^2)^{1/2} \sinh \eta^u\} \quad (8)$$

$u_{\perp} = \gamma v_{\perp} = \cosh \eta^u \gamma_{\perp} v_{\perp}$ ,  $\gamma_{\perp} = \cosh \rho^u$ . Due to the presence of non-zero azimuthal anisotropy, the azimuthal angle of the fluid velocity vector is not identical to the spatial azimuthal angle i.e.

$$u^{\mu}(x) = \{\gamma^{\phi} \cosh \rho'^u \cosh \eta^u, \sqrt{1 + \delta(b)} \sinh \rho'^u \cos \phi, \sqrt{1 - \delta(b)} \sinh \rho'^u \sin \phi, \cosh \rho'^u \sinh \eta^u\}$$

Where,

$$\gamma^{\phi} = \sqrt{1 + \delta(b) \tanh^2 \rho'^u \cos 2\phi}$$

$$\tan \phi^u = \sqrt{\frac{1 - \delta(b)}{1 + \delta(b)}} \tan \phi$$

The transverse flow rapidity  $\rho^u$  is related to  $\rho'^u$  as follows:

$$u_{\perp} = \sinh \rho^u = \sqrt{1 + \delta(b) \cos 2\phi} \sinh \rho'^u$$

We have used a simple rapidity linear profile for  $\rho'^u$  i.e

$$\rho_u = \frac{r}{R_f(b)} \rho_u^{max}(b=0) \quad (9)$$

where,  $r$  is the radial co-ordinate,  $\rho_u^{max}(b=0)$  is the maximum transverse flow rapidity in central collisions.  $R_f(b)$  is the mean-square radius of the hadron emission region.

In non-central collisions, the shape of the emission region in the  $x$ - $y$  plane can be approximated by an ellipse with semi-major axis  $R_y$  and semi-minor axis  $R_x$  [30]. The magnitude of the  $R_f = \sqrt{(R_x^2 + R_y^2)}/2$ .  $R_x(b) = R_f \sqrt{1 - \epsilon(b)}$  and  $R_y(b) = R_f \sqrt{1 + \epsilon(b)}$ , where  $\epsilon(b) = \frac{R_y^2 - R_x^2}{R_y^2 + R_x^2}$ . From the ellipse equation follows the dependence of the transverse radius of the hadron emission region on  $\phi$

$$R(b, \phi) = R_f(b) \frac{\sqrt{1 - \epsilon^2(b)}}{\sqrt{1 + \epsilon(b) \cos 2\phi}} \quad (10)$$

Here,  $\epsilon$  is the spatial anisotropy.

The effective volume of the hadron emission region for hypersurface of proper time  $\tau$  is calculated as follows:

$$V_{eff} = \tau \int_0^{2\pi} d\phi \int_0^{R(b, \phi)} (n_{\mu} n^{\mu}) r dr \int_{\eta_{min}}^{\eta_{max}} f(\eta) d\eta$$

Where  $(n_{\mu} n^{\mu}) = \cosh \rho_u \sqrt{1 + \delta(b) \tanh^2 \rho_u \cos 2\phi}$  and  $f(\eta)$  is the longitudinal rapidity profile (assumed uniform for this work) and  $\eta_{max}$  is the maximal longitudinal flow rapidity.

Elliptic flow is a result of pressure gradient in the overlap region. The expansion would be stronger along the

reaction plane where the pressure gradient is larger. Due to this expansion, the initial spatial anisotropy keeps changing [32]. Since the model does not trace the evolution of spatial anisotropy, we have only used the spatial anisotropy at thermal freeze-out. The initial spatial anisotropy depends on the impact parameter and nuclear geometry. Hence we have assumed a simple scaling between the eccentricity of the elliptical overlap region ( $\epsilon_0 = b/2R_A$ ) and the spatial anisotropy at thermal freeze-out i.e.

$$\epsilon = k \epsilon_0 \quad (11)$$

The parameter "k" is a scaling factor that indicates the change in azimuthal spatial anisotropy during evolution. The parameters  $\delta$  and  $\epsilon$  are related to each other by their dependence  $v_2$ , an empirical relation between the parameters estimated by the hydro-dynamical approach in the corresponding paper [5]:

$$v_2 \propto \frac{2(\delta - \epsilon)}{(1 - \delta^2)(1 - \epsilon^2)} \quad (12)$$

Using the fact that  $v_2 \propto \epsilon_0$  and  $\epsilon \propto \epsilon_0$  the relation between  $\epsilon$  and  $\delta$  can be calculated using eq. (12),

$$\delta = \frac{\sqrt{1 + 4B(\epsilon + B)} - 1}{2B}, B = C(1 - \epsilon^2)\epsilon \quad (13)$$

In this work, we have fixed the value of  $C = 2$ , and the value of scaling factor  $k$  is chosen to get the best match with the experimental data.

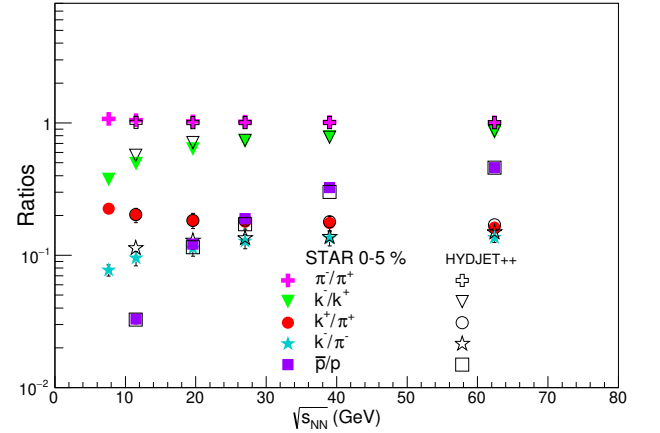


FIG. 1. Particle ratios at different beam energies.

Besides the above-synchronized formalism, the HYDJET++ model also has certain limitations. HYDJET++ model gives good results for the central and semi-central collision events but it fails to give convincing results for the peripheral collisions. The model can only be used for symmetric collisions (i.e. both the colliding nuclei should be of the same element). It works reliably for relatively heavier nuclei with nuclear mass  $A > 40$ . The model best

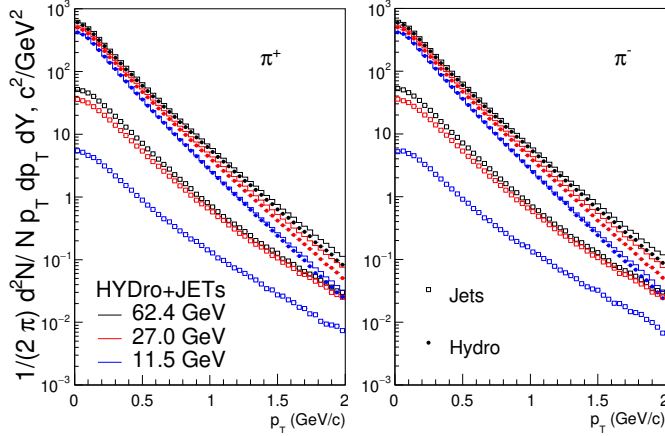


FIG. 2. Contributions from hydro and jet for  $\pi^\pm$ .

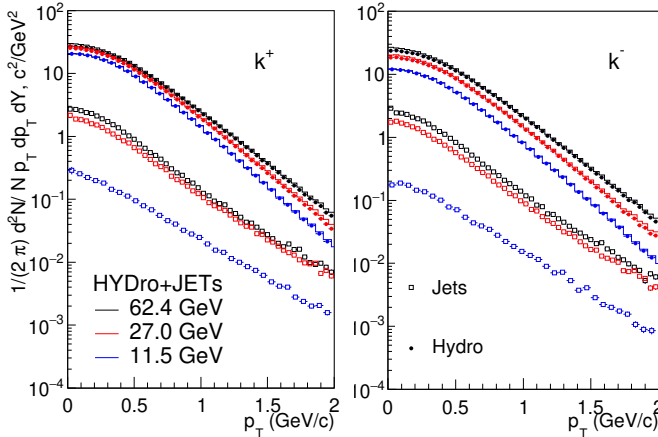


FIG. 3. Contributions from hydro and jet for  $k^\pm$ .

describes the experimental data in the mid-rapidity region. Another limitation of the HYDJET++ model is that it should be used for  $\sqrt{s_{NN}} > 10$  GeV. For the limitations described above we have chosen to limit our results up to 11.5 GeV and presented all our results in the mid-rapidity region.

### III. RESULTS AND DISCUSSIONS

We have simulated Au-Au collisions at a center of mass energies 62.4 GeV, 39.0 GeV, 27.0 GeV, 19.6 GeV, and 11.5 GeV using the HYDJET++ event generator and compared our results with the experimental data from STAR and PHENIX detectors. The kinematic range of our results is kept the same as the experimental data. The rapidity range for particle ratios and  $p_T$  spectra is  $|y| \leq 0.1$  and for  $v_2$  rapidity range is  $|y| \leq 0.35$  for PHENIX data and  $|y| \leq 1.0$  for STAR data. The exact

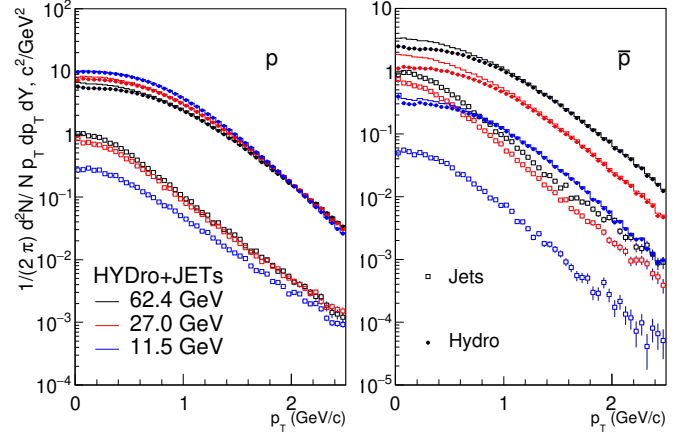


FIG. 4. Contributions from hydro and jet for  $p$  and  $\bar{p}$ .

number of events can be found in Table I.

TABLE I. The number of events for each centrality class.

$\sqrt{s_{NN}}$ (GeV)	0-5%	10-20%	30-40%	50-60%
62.4	$1.5 \times 10^5$	$2.0 \times 10^5$	$2.5 \times 10^5$	$2.0 \times 10^5$
39.0	$2.0 \times 10^5$	$2.5 \times 10^5$	$3.0 \times 10^5$	$5.0 \times 10^5$
27.0	$2.0 \times 10^5$	$3.5 \times 10^5$	$5.0 \times 10^5$	$7.0 \times 10^5$
19.6	$3.0 \times 10^5$	$4.5 \times 10^5$	$5.0 \times 10^5$	$7.0 \times 10^5$
11.5	$5.0 \times 10^5$	$7.0 \times 10^5$	$8.0 \times 10^5$	$1.0 \times 10^6$

The values of freeze-out parameters such as  $T_{ch}, \mu_B$ , and  $\mu_s$  used for this work are in agreement with the THERMUS model fit. A detailed analysis with the THERMUS model can be found in the corresponding papers [19, 33]. The exact values of input parameters used for this work can be found in Table II.

#### A. Particle Ratios

Fig. 1 shows HYDJET++ results for  $\pi^-/\pi^+, k^-/k^+, k^+/\pi^+, k^-/\pi^-$  and  $\bar{p}/p$  ratios at various center of mass energies for most central collisions at mid rapidity. The  $\pi^-/\pi^+$  ratio increases at lower collision energies but still remains close to 1. The  $k^-/k^+$  ratio increases with beam energy and approaches unity at  $\sqrt{s_{NN}} = 62.4$  GeV. The  $\bar{p}/p$  ratio also increases with beam energy, but the increase is more rapid than  $k^-/k^+$ . The  $k^+/\pi^+$  ratios decrease with increasing beam energy while the  $k^-/\pi^-$  ratio shows the opposite trend. Both these ratios become the same after 62.4 GeV due to smaller values of  $\mu_s$  at higher collision energies. The model calculations agree well with the experimental data with a slight deviation at 11.5 GeV.

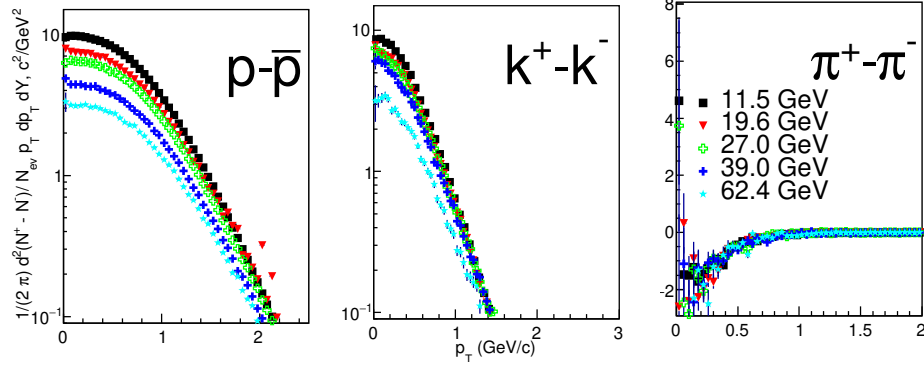


FIG. 5. Difference in invariant yield of particles and antiparticles as a function of beam energy.

TABLE II. The values of input model parameters for different beam energies.

$\sqrt{s_{NN}}$ (GeV)	$T_{ch}$ (GeV)	$\mu_B$ (GeV)	$\mu_s$ (GeV)	$T_{th}$ (GeV)	$\mu_{\pi}^{eff}$ (GeV)	$\eta^{max}$	$\rho_u^{max}$
62.4	0.165	0.0725	0.015	0.095	0.082	2.6	0.96
39.0	0.164	0.112	0.028	0.092	0.088	2.1	0.94
27.0	0.1625	0.156	0.033	0.091	0.0962	1.9	0.93
19.6	0.160	0.192	0.038	0.089	0.1	1.85	0.92
11.5	0.1526	0.268	0.055	0.085	0.1005	1.7	0.91

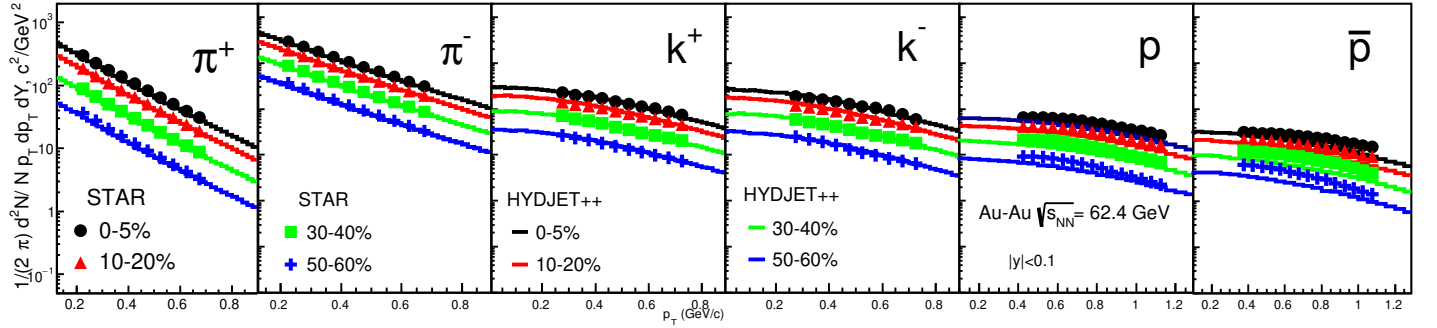


FIG. 6. Transverse momentum spectra for different centralities at  $\sqrt{s_{NN}} = 62.4$  GeV. Markers represent experimental data and HYDJET++ results are shown as lines.

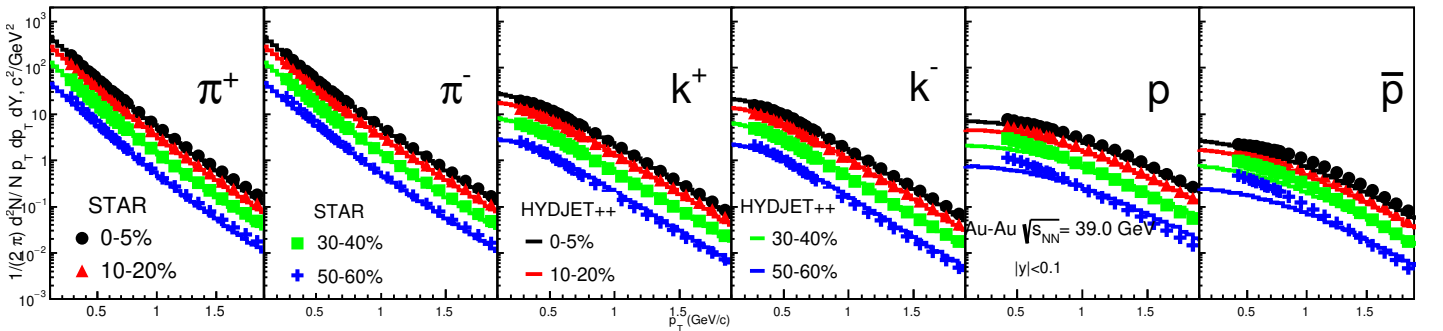


FIG. 7. Transverse momentum spectra for different centralities at  $\sqrt{s_{NN}} = 39.0$  GeV. Markers represent experimental data and HYDJET++ results are shown as lines.

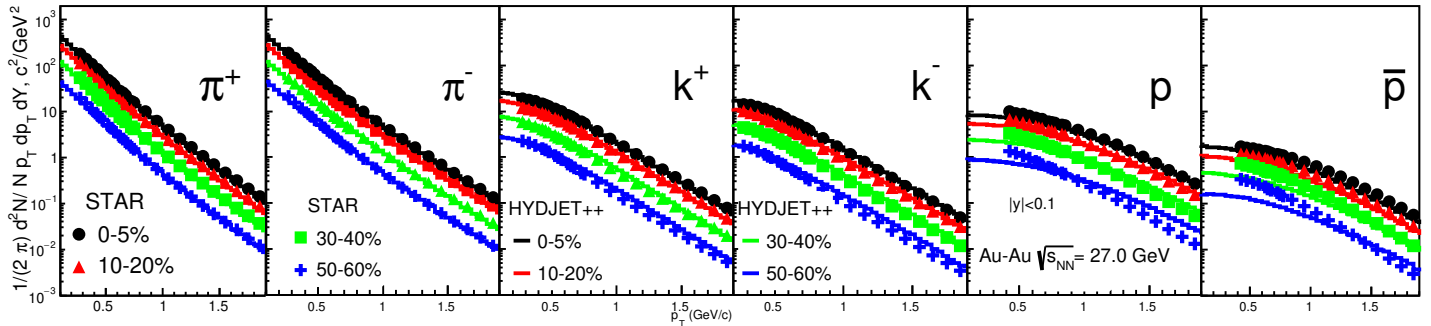


FIG. 8. Transverse momentum spectra for different centralities at  $\sqrt{s_{NN}} = 27.0$  GeV. Markers represent experimental data and HYDJET++ results are shown as lines.

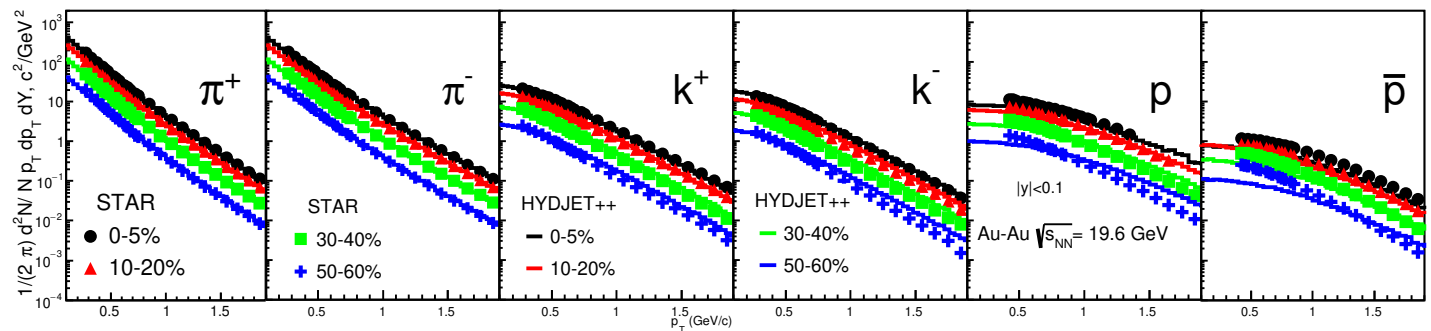


FIG. 9. Transverse momentum spectra for different centralities at  $\sqrt{s_{NN}} = 19.6$  GeV. Markers represent experimental data and HYDJET++ results are shown as lines.

### B. $p_T$ spectra

In the HYDJET++ framework, the particles are produced as a combination of a hydro part and jets. So, It is crucial to check the contribution from both processes. Fig. 2 shows the contributions from hydro and jets in  $p_T$  spectra of  $\pi^\pm$  for most central collisions for  $\sqrt{s_{NN}} = 62.4, 27.0$  and  $11.5$  GeV. It is evident that the hydro part predominates the  $p_T$  spectra at low  $p_T$ , and the contribution from jets starts to affect the overall form of  $p_T$  spectra at relatively higher  $p_T$ . It's worth noting that the contributions from both processes drop with decreasing beam energy. However, the contribution from jets decreases more rapidly than that of the hydro part. In Fig. 3 we have shown the effect of both processes for  $k^\pm$ , the contributions are similar to that of charged pions, however for  $k^-$  the contributions from the soft part decrease more rapidly with decreasing beam energy than  $k^+$ . The effects from hydro and jets for  $p$  and  $\bar{p}$  are shown in Fig. 4. In the  $p_T$  spectra of protons, the contributions from jets decrease with decreasing beam energy while the contributions from the hydro part increase rapidly. As a result the overall contribution increases. This can be attributed to an increase in baryon density at lower collision energies [19]. For  $\bar{p}$  contributions from both processes decrease rapidly with decreasing beam energy. We have discussed

the difference in  $p_T$  of particles and antiparticles later. A similar analysis for Au-Au collisions at 200 GeV using the HYDJET++ model for kaons and pions can be found in the corresponding papers [24, 25].

A clear beam energy dependence is observed in the difference in the invariant yields of  $p$  and  $\bar{p}$ . The difference increases with the decrease in beam energy. This is due to the increase in chemical potential which determines the difference between the number of particles and antiparticles [34, 35], the effect of chemical potential is clearly observed in the soft part of the  $p_T$  spectra. However, the contribution from jets makes the difference relatively negligible beyond  $p_T \approx 1.5$  GeV/c. Similar trends are seen for  $k^\pm$  as well, but they are less pronounced in comparison to  $p$  and  $\bar{p}$  because of the smaller values of strangeness chemical potential compared to baryonic chemical potential. Charged pions that have negative chemical potential show an opposite trend at low  $p_T$  ( $p_T \leq 1$  GeV/c). A detailed comparison can be seen in Fig. 5.

In Fig. 6 to Fig. 10 we have shown the transverse momentum spectra at low  $p_T$  for different beam energies. Our results are shown in four centrality classes i.e. (0-5)%, (10-20)%, (30-40)%, and (50-60)%. For comparison, we have shown the experimental data from STAR [19, 36]. The  $p_T$  spectra of  $\pi^\pm$  and  $k^\pm$  show a good match with the experimental data in central and semi-central colli-

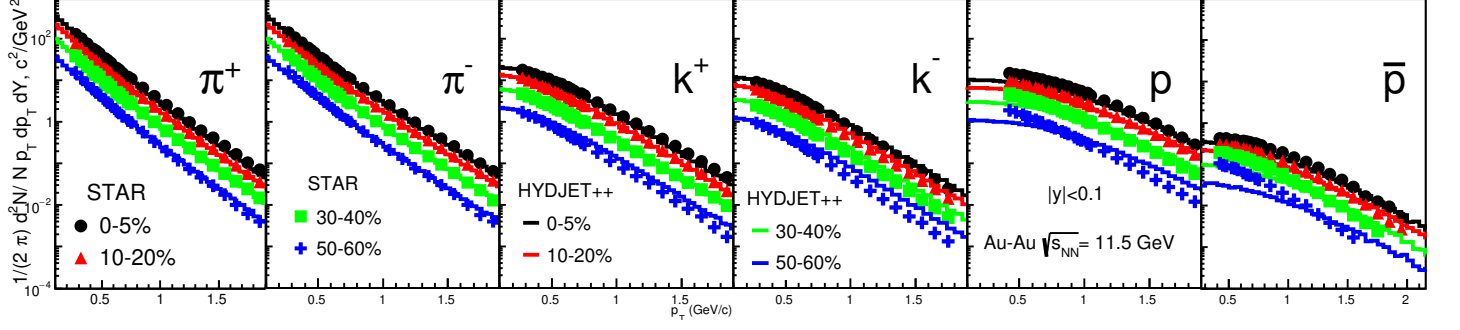


FIG. 10. Transverse momentum spectra for different centralities at  $\sqrt{s_{NN}} = 11.5$  GeV. Markers represent experimental data and HYDJET++ results are shown as lines.

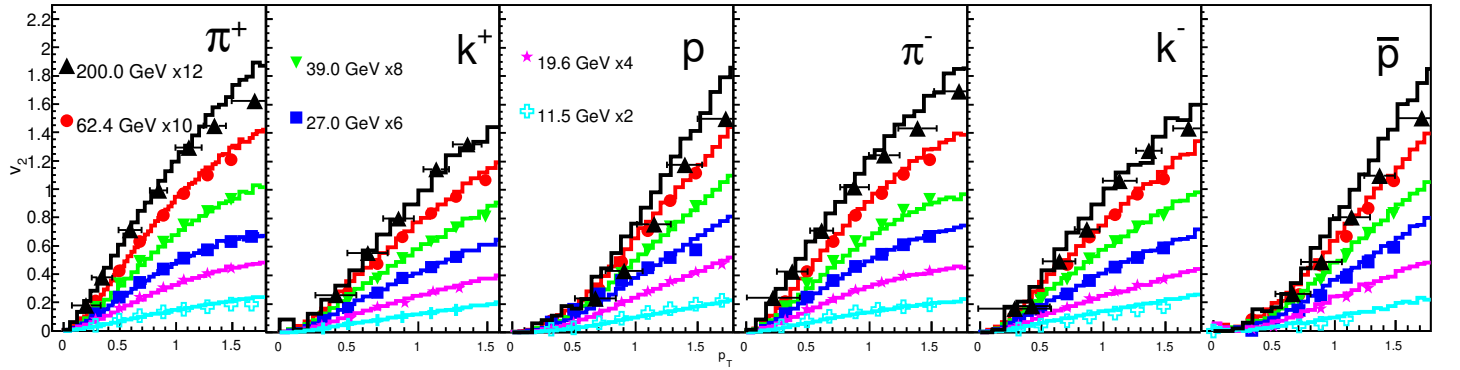


FIG. 11.  $v_2$  at different collision energies. Markers represent experimental data. Lines of the same color show HYDJET++ results.

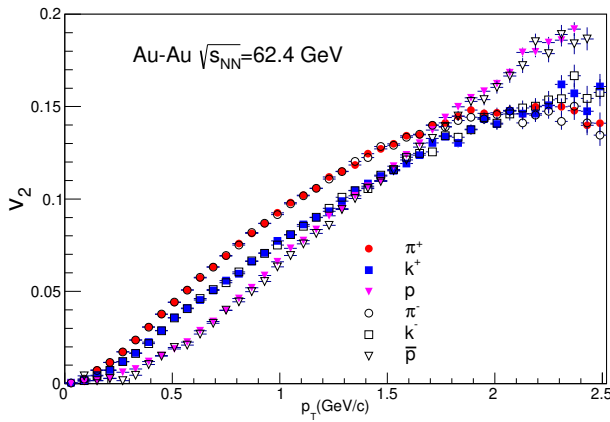


FIG. 12.  $v_2$  of primary hadrons at  $\sqrt{s_{NN}} = 62.4$  GeV.

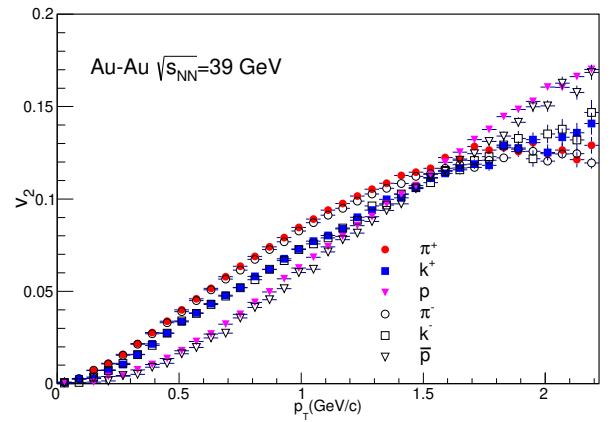


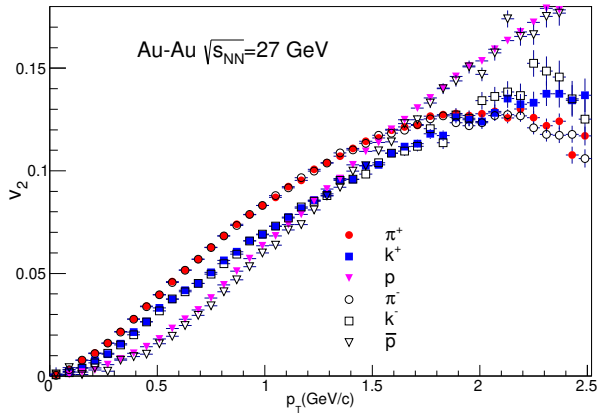
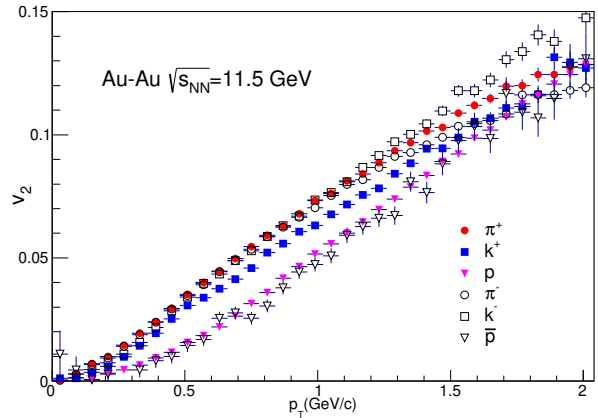
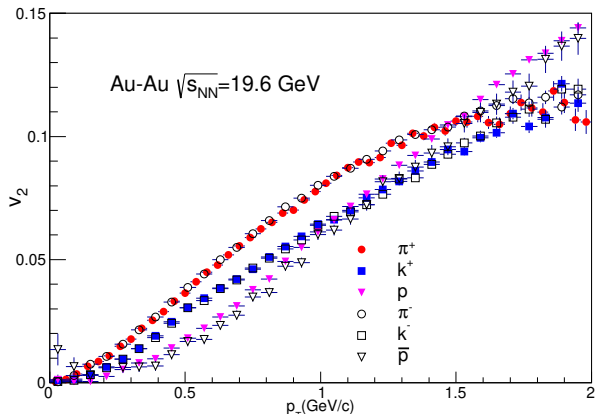
FIG. 13.  $v_2$  of primary hadrons at  $\sqrt{s_{NN}} = 39.0$  GeV.

tion while the model slightly over-predict  $k^\pm$  at peripheral collisions for lower beam energies. The model under-predicts the  $p_T$  spectra of  $p$  and  $\bar{p}$  up to  $p_T = 0.5$  GeV/ $c$  after  $0.5$  GeV/ $c$  there is a good match. The results for peripheral collisions at lower beam energy show a clear

mismatch with the experimental data. This is due to a strong centrality dependence of  $\mu_B$  which is observed at  $11.5$  and  $19.6$  GeV [19].

The invariant yield tends to decrease from central to peripheral collisions. This behavior is the same for all



FIG. 14.  $v_2$  of primary hadrons at  $\sqrt{s_{NN}}=27.0$  GeV.FIG. 16.  $v_2$  of primary hadrons at  $\sqrt{s_{NN}}=11.5$  GeV.FIG. 15.  $v_2$  of primary hadrons at  $\sqrt{s_{NN}}=19.6$  GeV.

particles. There is no beam energy dependence of variation of  $p_T$  spectra with collision centrality observed in our model calculations. The centrality dependence at lower collision energies is similar to the one observed for the top RHIC energy as well as LHC energies [37, 38].

### C. Elliptic flow ( $v_2$ )

In non-central heavy ion collisions, the initial asymmetry of the collision results in a higher pressure gradient along the reaction plane compared to directions out of this plane. One of the major aspects of the particles produced inside the QGP medium of the off-centered collisions is that more particles are emitted along the reaction plane than perpendicular to it [39–41]. Such a phenomenon is called the elliptic flow. The magnitude of elliptic flow is given by

$$v_2 = \cos(2\phi) \quad (14)$$

where  $\phi$  is the spatial azimuthal angle and the reaction plane angle is taken 0.

The heavier quarks like charm and beauty interact with the QGP medium and experience a drag, which affects their transport coefficients. This leads to a mass-dependent pertinent elliptic flow of the heavy quarks at the end of the QGP phase [42, 43]. A similar phenomenon is possible for the strange quarks at BES energies due to the lower temperatures of these systems. Hence, in this work, we have treated the strange and non-strange hadrons differently to check the impact of quark content on the scaling factor "k".

In Fig . 11 we have presented the HYDJET++ model calculations for  $v_2$  as a function of  $p_T$  for the center of mass energy  $\sqrt{s_{NN}} = 200.0, 62.4, 39.0, 27.0, 19.6$  and  $11.5$  GeV for minimum bias collisions (0-80%). For clear representation we have scaled  $v_2$  of all energies by a different factor, the exact weights for scaling can be found in the legend. The results are compared with the experimental data from STAR [18] and PHENIX [44] experiments. HYDJET++ calculations agree well with the experimental data [18, 44] up to  $p_T = 2$  GeV/c at mid-rapidity. The model overpredicts the  $v_2$  of  $p$  and  $\bar{p}$  at 200 GeV, it also overpredicts the  $v_2$  of  $k^-$  at 11.5 GeV. The  $v_2$  increases with  $p_T$  for all collision energy and reaches a maximum value of approximately 0.15 for mesons and 0.2 for baryons, the maximum value decreases with decreasing beam energy. It should be noted that  $v_2$  at low  $p_T$  (i.e.  $p_T \leq 1$  GeV/c) is independent of collision energy, the effect of collision is observed after 1 GeV/c as  $v_2$  approaches its maximum value. The elliptic flow( $v_2$ ) at lower  $p_T$  ( $p_T < 1.5$  GeV/c) shows a dependence on the mass of the particle species. The particles with lower mass have a larger value of  $v_2$  i.e. ( $v_2(\pi^+) > v_2(k^+) > v_2(p)$ ). A similar trend is also observed for corresponding anti-particles [45, 46]. A mass ordering in  $v_2$  has been observed in the Au-Au collision at 200 GeV [47, 48]. Recent experiments like RHIC BES have also observed a mass ordering in  $v_2$  at lower colli-



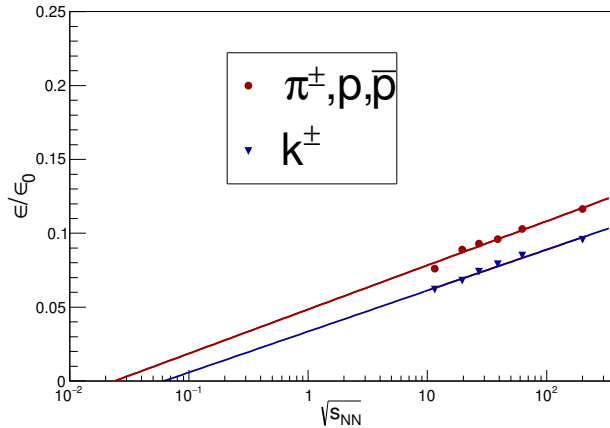


FIG. 17. Relation between scaling factor  $k$  and beam energy. Lines show the fitting function from eq. (15).

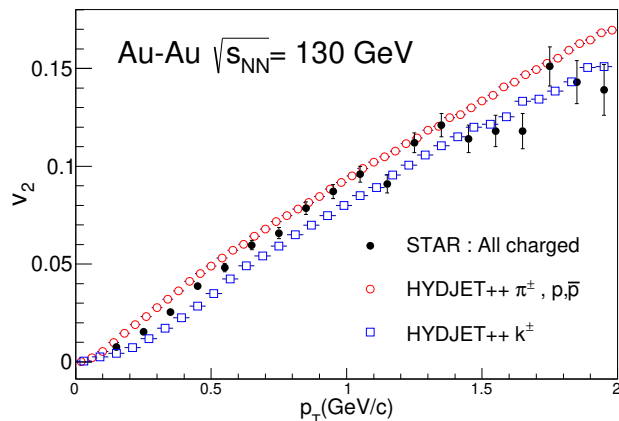


FIG. 18.  $v_2$  as a function of  $p_T$  for  $\sqrt{s_{NN}} = 130$  GeV.

sion energies [18]. To validate our approach of treating strange and non-strange hadrons separately, we should check for mass ordering in our calculations. In Fig. 12 to Fig. 16 we have shown  $v_2$  as a function of  $p_T$  for  $\sqrt{s_{NN}} = 62.4, 39.0, 27.0, 19.6,$  and  $11.5$  GeV. The  $v_2$  of all the particles are plotted together for a clear comparison. The  $v_2$  of particles are represented by solid markers and the  $v_2$  of antiparticles are shown by open markers to get an idea about the difference in  $v_2$  of particles and antiparticles, more details can be found in the legend. A clear mass ordering can be seen in the HYDJET++ calculation in all five collision energies. Mass ordering is observed up to  $p_T = 1.5$  GeV/c. After 1.5 GeV/c the  $v_2$  of protons increases rapidly and surpasses the  $v_2$  of pions and kaons. At about 2 GeV/c an opposite trend is observed i.e ( $v_2(\pi^+) < v_2(k^+) < v_2(p)$ ). For  $\pi^\pm$  and  $k^\pm$  the  $v_2$  is the same for both particles and anti-particles, while at 11.5 GeV  $k^-$  has a higher  $v_2$  than  $k^+$ . Protons have relatively larger  $v_2$  than the anti-protons at all collision energies.

We have found that the value of scaling factor  $k$  in minimum bias collisions has the following relation with beam energy.

$$k = a \ln(\sqrt{s_{NN}}) + b \quad (15)$$

where, for  $\pi^\pm$  and  $p\bar{p}$   
 $a = 0.0129 \pm 0.001$ ,  $b = 0.0485 \pm 0.004$ ,  
and, for  $k^\pm$   
 $a = 0.012 \pm 0.0007$ ,  $b = 0.0335 \pm 0.002$ .

The value of  $a$  is almost the same for all particles, while the value of  $b$  for non-strange hadrons is greater than the strange hadrons. It indicates that in the HYDJET++ framework, the magnitude of azimuthal spatial and momentum anisotropy (which determines the elliptic flow ( $v_2$ )) is dependent on quark content, which suggests that the strange quarks also experience a drag inside the QGP similar to the charm and beauty quarks. The collective behavior is weaker for the lower energies of the Beam Energy Scan range. Hence, the particles are emitted uniformly in all directions [49] which reduces their spatial and momentum anisotropy which reflects as a reduced "k" value [50]. A clear depiction can be found in Fig. 17.

Our analysis of  $v_2$  shows a trend in variation of  $k$  with beam energy as discussed earlier. We have studied the top RHIC energy of 200 GeV and the lower energies. It is essential to verify this trend at intermediate collision energy. We have chosen 130 GeV as the intermediate energy. In Fig. 18 we have shown  $v_2$  as a function of  $p_T$  for minimum bias collisions (0-80%) at  $\sqrt{s_{NN}} = 130$  GeV. The input value of  $k$  is taken according to eq. (15), and  $\delta$  and  $\epsilon$  are calculated accordingly. The baryonic chemical potential and chemical freezeout temperatures are taken according to eq. (3). The rest input parameters are same as default values for  $\sqrt{s_{NN}} = 200$  GeV. The combined elliptic flow of non-strange hadrons ( $\pi^\pm$  and  $p, \bar{p}$ ) are represented with red markers, and the combined  $v_2$  of  $k^\pm$  is shown with blue markers. The  $v_2$  of  $\pi^\pm$  and  $p, \bar{p}$  is higher than the combined flow of charged kaons ( $k^\pm$ ). This is due to the higher value of  $\epsilon$  for non-strange hadrons than strange ones which leads to a higher combined  $v_2$ . The results are compared with the combined  $v_2$  of charged hadrons measured experimentally by the STAR detector [51].

#### IV. SUMMARY

We have performed a comprehensive study of bulk properties of medium like  $p_T$  spectra and elliptic flow produced in Au-Au collisions at different beam energies. HYDJET++ model shows a good match with the experimentally observed particle ratios with suitable chemical potentials and chemical freezeout temperatures. HYDJET++ calculations of  $p_T$  spectra show a good match with experimental data for central and semi-central collisions. The model slightly under-predicts  $p_T$  spectra of

$p$  and  $\bar{p}$ . The contribution of hard and soft processes decreases with decreasing beam energy. The contributions from the hard part decrease more rapidly than the soft part, at lower energies like 11.5 GeV  $p_T$  spectra is entirely determined by the soft processes. The contribution of the soft part in the invariant yield of protons shows an opposite trend, it increases with decreasing beam energy.

HYDJET++ results on elliptic flow show a good match with experimental data. The model calculations as well as the experimental show a beam energy dependence of  $v_2$  after 1 GeV/c, the  $v_2$  in these regions increases with beam energy. No beam energy dependence is seen for  $p_T < 1$  GeV/c. In the regime of low  $p_T$ , a mass ordering in  $v_2$  is also observed in our model calculations i.e. ( $v_2(\pi^+) > v_2(k^+) > v_2(p)$ ), this trend is also seen for the anti-particles. The mass ordering is not observed after 1.5 GeV/c. The difference between  $v_2$  of particles and anti-particles is not observed for mesons, while a

slight difference in  $v_2$  is seen for  $p$  and  $\bar{p}$  ( $v_2(p) > v_2(\bar{p})$ ). The azimuthal spatial anisotropy increases with collision energy as shown in eq. (15). The azimuthal spatial anisotropy ( $\epsilon$ ) at a given collision energy is the same for  $\pi^\pm, p$  and  $\bar{p}$ , while the charged kaons have a lesser value of  $\epsilon$ , which suggests that the relatively heavier strange quarks interact with the QGP medium and experience a drag that affects the final spatial and momentum anisotropy of strange hadrons.

## ACKNOWLEDGMENTS

BKS sincerely acknowledges financial support from the Institute of Eminence (IoE) BHU Grant number 6031. SRN acknowledges the financial support from the UGC Non-NET fellowship during the research work. SP acknowledges the financial support obtained from UGC and IoE under a research fellowship scheme during the work.

- 
- [1] J. C. Collins and M. J. Perry, Phys. Rev. Lett. **34** (1975), 1353 doi:10.1103/PhysRevLett.34.1353
- [2] N. Cabibbo and G. Parisi, “Exponential Hadronic Spectrum and Quark Liberation,” Phys. Lett. B **59** (1975), 67-69 doi:10.1016/0370-2693(75)90158-6
- [3] G. Chapline and M. Nauenberg, “Asymptotic Freedom and the Baryon-Quark Phase Transition,” Phys. Rev. D **16** (1977), 450 doi:10.1103/PhysRevD.16.450
- [4] C. P. Singh Signals of quark-gluon plasma. *Physics Reports*. **236**, 147-224 (1993)
- [5] U. A. Wiedemann, “Two particle interferometry for noncentral heavy ion collisions,” Phys. Rev. C **57** (1998), 266-279 doi:10.1103/PhysRevC.57.266 [arXiv:nucl-th/9707046 [nucl-th]].
- [6] K. Adcox *et al.* [PHENIX], “Suppression of hadrons with large transverse momentum in central Au+Au collisions at  $\sqrt{s_{NN}} = 130$ -GeV,” Phys. Rev. Lett. **88** (2002), 022301 doi:10.1103/PhysRevLett.88.022301 [arXiv:nucl-ex/0109003 [nucl-ex]].
- [7] J. Rafelski and B. Muller, “Strangeness Production in the Quark - Gluon Plasma,” Phys. Rev. Lett. **48** (1982), 1066 [erratum: Phys. Rev. Lett. **56** (1986), 2334] doi:10.1103/PhysRevLett.48.1066
- [8] J. Rafelski, “Formation and Observables of the Quark-Gluon Plasma,” Phys. Rept. **88** (1982), 331 UFTP-80-1982.
- [9] C. Y. Wong, “J / psi suppression as a signal for the quark gluon plasma,” [arXiv:hep-ph/9712332 [hep-ph]].
- [10] F. Becattini, J. Manninen and M. Gazdzicki, “Energy and system size dependence of chemical freeze-out in relativistic nuclear collisions,” Phys. Rev. C **73** (2006), 044905 doi:10.1103/PhysRevC.73.044905 [arXiv:hep-ph/0511092 [hep-ph]].
- [11] A. Andronic, P. Braun-Munzinger and J. Stachel, “Hadron production in central nucleus-nucleus collisions at chemical freeze-out,” Nucl. Phys. A **772** (2006), 167-199 doi:10.1016/j.nuclphysa.2006.03.012 [arXiv:nucl-th/0511071 [nucl-th]].
- [12] J. Cleymans and K. Redlich, “Chemical and thermal freezeout parameters from 1-A/GeV to 200-A/GeV,” Phys. Rev. C **60** (1999), 054908 doi:10.1103/PhysRevC.60.054908 [arXiv:nucl-th/9903063 [nucl-th]].
- [13] Fodor, Z. & Katz, S. Critical point of QCD at finite T and mu, lattice results for physical quark masses. *JHEP*. **4** pp. 050 (2004)
- [14] R. V. Gavai and S. Gupta, “QCD at finite chemical potential with six time slices,” Phys. Rev. D **78** (2008), 114503 doi:10.1103/PhysRevD.78.114503 [arXiv:0806.2233 [hep-lat]].
- [15] L. Adamczyk *et al.* [STAR], “Collision Energy Dependence of Moments of Net-Kaon Multiplicity Distributions at RHIC,” Phys. Lett. B **785** (2018), 551-560 doi:10.1016/j.physletb.2018.07.066 [arXiv:1709.00773 [nucl-ex]].
- [16] J. Adam *et al.* [STAR], “Collision-energy dependence of second-order off-diagonal and diagonal cumulants of net-charge, net-proton, and net-kaon multiplicity distributions in Au + Au collisions,” Phys. Rev. C **100** (2019) no.1, 014902 [erratum: Phys. Rev. C **105** (2022) no.2, 029901] doi:10.1103/PhysRevC.100.014902 [arXiv:1903.05370 [nucl-ex]].
- [17] B. Mohanty, “QCD Phase Diagram: Phase Transition, Critical Point and Fluctuations,” Nucl. Phys. A **830** (2009), 899C-907C doi:10.1016/j.nuclphysa.2009.10.132 [arXiv:0907.4476 [nucl-ex]].
- [18] L. Adamczyk *et al.* [STAR], “Elliptic flow of identified hadrons in Au+Au collisions at  $\sqrt{s_{NN}} = 7.7$ -62.4 GeV,” Phys. Rev. C **88** (2013), 014902 doi:10.1103/PhysRevC.88.014902 [arXiv:1301.2348 [nucl-ex]].
- [19] L. Adamczyk *et al.* [STAR], “Bulk Properties of the Medium Produced in Relativistic Heavy-Ion Collisions from the Beam Energy Scan Program,” Phys. Rev. C **96** (2017) no.4, 044904 doi:10.1103/PhysRevC.96.044904 [arXiv:1701.07065 [nucl-ex]].
- [20] B. I. Abelev *et al.* [STAR], “Identified particle production, azimuthal anisotropy, and interferometry

- measurements in Au+Au collisions at  $\sqrt{s(NN)}^{1/2} = 9.2$  GeV,” *Phys. Rev. C* **81** (2010), 024911 doi:10.1103/PhysRevC.81.024911 [arXiv:0909.4131 [nucl-ex]].
- [21] D. Solanki, P. Sorensen, S. Basu, R. Raniwala and T. K. Nayak, “Beam energy dependence of Elliptic and Triangular flow with the AMPT model,” *Phys. Lett. B* **720** (2013), 352-357 doi:10.1016/j.physletb.2013.02.028 [arXiv:1210.0512 [nucl-ex]].
- [22] M. Nasim, L. Kumar, P. K. Netrakanti and B. Mohanty, “Energy dependence of elliptic flow from heavy-ion collision models,” *Phys. Rev. C* **82** (2010), 054908 doi:10.1103/PhysRevC.82.054908 [arXiv:1010.5196 [nucl-ex]].
- [23] I. P. Lokhtin, L. V. Malinina, S. V. Petrushanko, A. M. Snigirev, I. Arsene and K. Tywoniuk, “HYD-JET++ heavy ion event generator and its applications for RHIC and LHC,” *PoS High-pT physics09* (2009), 023 doi:10.22323/1.080.0023 [arXiv:0903.0525 [hep-ph]].
- [24] I. P. Lokhtin, L. V. Malinina, S. V. Petrushanko, A. M. Snigirev, I. Arsene and K. Tywoniuk, “Heavy ion event generator HYDJET++ (HYDrodynamics plus JETs),” *Comput. Phys. Commun.* **180** (2009), 779-799 doi:10.1016/j.cpc.2008.11.015 [arXiv:0809.2708 [hep-ph]].
- [25] A. Singh, P. K. Srivastava, G. Devi and B. K. Singh, “Production and enhancement of (multi-) strange hadrons in Au+Au collisions at  $\sqrt{sNN}=200$  GeV RHIC energy and Pb+Pb collisions at  $\sqrt{sNN}=2.76$  TeV LHC energy,” *Phys. Rev. C* **107** (2023) no.2, 024906 doi:10.1103/PhysRevC.107.024906
- [26] I. P. Lokhtin, L. V. Malinina, S. V. Petrushanko and A. M. Snigirev, “HYDJET++ model of relativistic heavy-ion collisions,” *Phys. Atom. Nucl.* **73** (2010), 2139-2147 doi:10.1134/S1063778810120203
- [27] T. Sjostrand, S. Mrenna and P. Z. Skands, “PYTHIA 6.4 Physics and Manual,” *JHEP* **05** (2006), 026 doi:10.1088/1126-6708/2006/05/026 [arXiv:hep-ph/0603175 [hep-ph]].
- [28] K. Tywoniuk, I. Arsene, L. Bravina, A. Kaidalov and E. Zabrodin, “Gluon shadowing in the Glauber-Gribov model at HERA,” *Phys. Lett. B* **657** (2007), 170-175 doi:10.1016/j.physletb.2007.09.065 [arXiv:0705.1596 [hep-ph]].
- [29] N. S. Amelin, R. Lednicky, T. A. Pocheptsov, I. P. Lokhtin, L. V. Malinina, A. M. Snigirev, I. A. Karpenko and Y. M. Sinyukov, “A Fast hadron freeze-out generator,” *Phys. Rev. C* **74** (2006), 064901 doi:10.1103/PhysRevC.74.064901 [arXiv:nucl-th/0608057 [nucl-th]].
- [30] N. S. Amelin, R. Lednicky, I. P. Lokhtin, L. V. Malinina, A. M. Snigirev, I. A. Karpenko, Y. M. Sinyukov, I. Arsene and L. Bravina, “Fast hadron freeze-out generator. Part II. Noncentral collisions,” *Phys. Rev. C* **77** (2008), 014903 doi:10.1103/PhysRevC.77.014903 [arXiv:0711.0835 [hep-ph]].
- [31] G. D. Yen, M. I. Gorenstein, W. Greiner and S. N. Yang, “Excluded volume hadron gas model for particle number ratios in A+A collisions,” *Phys. Rev. C* **56** (1997), 2210-2218 doi:10.1103/PhysRevC.56.2210 [arXiv:nucl-th/9711062 [nucl-th]].
- [32] P. F. Kolb, J. Sollfrank and U. W. Heinz, “Anisotropic flow from AGS to LHC energies,” *Phys. Lett. B* **459** (1999), 667-673 doi:10.1016/S0370-2693(99)00720-0 [arXiv:nucl-th/9906003 [nucl-th]].
- [33] V. Vovchenko and H. Stoecker, “Thermal-FIST: A package for heavy-ion collisions and hadronic equation of state,” *Comput. Phys. Commun.* **244** (2019), 295-310 doi:10.1016/j.cpc.2019.06.024 [arXiv:1901.05249 [nucl-th]].
- [34] D. Anchishkin, V. Gnatovskyy, D. Zhuravel and V. Karpenko, “Self-interacting particle-antiparticle system of bosons,” *Phys. Rev. C* **105** (2022) no.4, 045205 doi:10.1103/PhysRevC.105.045205 [arXiv:2102.02529 [nucl-th]].
- [35] J. Cleymans and K. Redlich, “Unified description of freezeout parameters in relativistic heavy ion collisions,” *Phys. Rev. Lett.* **81** (1998), 5284-5286 doi:10.1103/PhysRevLett.81.5284 [arXiv:nucl-th/9808030 [nucl-th]].
- [36] B. I. Abelev *et al.* [STAR], “Systematic Measurements of Identified Particle Spectra in  $pp, d^+$  Au and Au+Au Collisions from STAR,” *Phys. Rev. C* **79** (2009), 034909 doi:10.1103/PhysRevC.79.034909 [arXiv:0808.2041 [nucl-ex]].
- [37] S. Acharya *et al.* [ALICE], “Transverse momentum spectra and nuclear modification factors of charged particles in pp, p-Pb and Pb-Pb collisions at the LHC,” *JHEP* **11** (2018), 013 doi:10.1007/JHEP11(2018)013 [arXiv:1802.09145 [nucl-ex]].
- [38] A. Adare *et al.* [PHENIX], “Spectra and ratios of identified particles in Au+Au and d+Au collisions at  $\sqrt{s_{NN}} = 200$  GeV,” *Phys. Rev. C* **88** (2013) no.2, 024906 doi:10.1103/PhysRevC.88.024906 [arXiv:1304.3410 [nucl-ex]].
- [39] D. Kharzeev and M. Nardi, “Hadron production in nuclear collisions at RHIC and high density QCD,” *Phys. Lett. B* **507** (2001), 121-128 doi:10.1016/S0370-2693(01)00457-9 [arXiv:nucl-th/0012025 [nucl-th]].
- [40] R. Snellings, “Elliptic Flow: A Brief Review,” *New J. Phys.* **13** (2011), 055008 doi:10.1088/1367-2630/13/5/055008 [arXiv:1102.3010 [nucl-ex]].
- [41] A. M. Poskanzer and S. A. Voloshin, “Methods for analyzing anisotropic flow in relativistic nuclear collisions,” *Phys. Rev. C* **58** (1998), 1671-1678 doi:10.1103/PhysRevC.58.1671 [arXiv:nucl-ex/9805001 [nucl-ex]].
- [42] M. He, H. van Hees and R. Rapp, “Heavy-quark diffusion in the quark-gluon plasma,” *Prog. Part. Nucl. Phys.* **130** (2023), 104020 doi:10.1016/j.pnpnp.2023.104020 [arXiv:2204.09299 [hep-ph]].
- [43] R. Rapp, P. B. Gossiaux, A. Andronic, R. Averbeck, S. Masciocchi, A. Beraudo, E. Bratkovskaya, P. Braun-Munzinger, S. Cao and A. Dainese, *et al.* “Extraction of Heavy-Flavor Transport Coefficients in QCD Matter,” *Nucl. Phys. A* **979** (2018), 21-86 doi:10.1016/j.nuclphysa.2018.09.002 [arXiv:1803.03824 [nucl-th]].
- [44] S. S. Adler *et al.* [PHENIX], “Elliptic flow of identified hadrons in Au+Au collisions at  $\sqrt{s(NN)}^{1/2} = 200$ -GeV,” *Phys. Rev. Lett.* **91** (2003), 182301 doi:10.1103/PhysRevLett.91.182301 [arXiv:nucl-ex/0305013 [nucl-ex]].
- [45] P. Huovinen, P. F. Kolb, U. W. Heinz, P. V. Ruuskanen and S. A. Voloshin, “Radial and elliptic flow at RHIC: Further predictions,” *Phys. Lett. B* **503** (2001), 58-64 doi:10.1016/S0370-2693(01)00219-2 [arXiv:hep-ph/0101136 [hep-ph]].

- [46] P. Huovinen and P. V. Ruuskanen, “Hydrodynamic Models for Heavy Ion Collisions,” *Ann. Rev. Nucl. Part. Sci.* **56** (2006), 163-206 doi:10.1146/annurev.nucl.54.070103.181236 [arXiv:nucl-th/0605008 [nucl-th]].
- [47] B. I. Abelev *et al.* [STAR], “Centrality dependence of charged hadron and strange hadron elliptic flow from  $\sqrt{s_{NN}} = 200$ -GeV Au + Au collisions,” *Phys. Rev. C* **77** (2008), 054901 doi:10.1103/PhysRevC.77.054901 [arXiv:0801.3466 [nucl-ex]].
- [48] L. Adamczyk *et al.* [STAR], “Centrality dependence of identified particle elliptic flow in relativistic heavy ion collisions at  $\sqrt{s_{NN}}=7.7-62.4$  GeV,” *Phys. Rev. C* **93** (2016) no.1, 014907 doi:10.1103/PhysRevC.93.014907 [arXiv:1509.08397 [nucl-ex]].
- [49] M. Słodkowski, D. Setniewski, P. Aszklar and J. Porter-Sobieraj, “Modeling the Dynamics of Heavy-Ion Collisions with a Hydrodynamic Model Using a Graphics Processor,” *Symmetry* **13** (2021) no.3, 507 doi:10.3390/sym13030507
- [50] S. R. Nayak, S. Pandey and B. K. Singh, “Beam energy dependence of elliptic flow in Au-Au collisions using HY-DJET++ model,” *DAE Symp. Nucl. Phys.* **67** (2024), 1087-1088
- [51] K. H. Ackermann *et al.* [STAR], “Elliptic flow in Au + Au collisions at  $\sqrt{s_{NN}} = 130$  GeV,” *Phys. Rev. Lett.* **86** (2001), 402-407 doi:10.1103/PhysRevLett.86.402 [arXiv:nucl-ex/0009011 [nucl-ex]].